



## Article

# On the Surface Hardening of Zinc Sulfide Windows by Gallium Sulfide<sup>†</sup>

Hayat Soufiani<sup>1,\*</sup>, Alexandros Kostogiannes<sup>1</sup>, Clara Rivero-Baleine<sup>2</sup>, Kathleen A. Richardson<sup>1</sup> and Romain Gaume<sup>1,\*</sup>

<sup>1</sup> CREOL, The College of Optics and Photonics, University of Central Florida, 4304 Scorpius St., Orlando, FL 32816, USA; alexandros.kostogiannes@ucf.edu (A.K.); kcr@creol.ucf.edu (K.A.R.)

<sup>2</sup> Lockheed Martin Corporation, 5600 Sand Lake Rd., Orlando, FL 32819, USA; clara.rivero-baleine@creol.ucf.edu

\* Correspondence: hayat.soufiani@ucf.edu (H.S.); gaume@ucf.edu (R.G.)

<sup>†</sup> This paper in an expanded version of “Solute strengthening of multispectral ZnS windows by vapor transport of Ga<sub>2</sub>S<sub>3</sub>”. In Proceedings of the Window and Dome Technologies and Materials XVII, Orlando, FL, USA, 4 May 2023.

**Abstract:** This study examines the effect of gallium doping on the phase transformation, transmission, and hardness of commercial multispectral-grade ZnS specimens exposed to Ga<sub>2</sub>S<sub>3</sub> vapor. Using secondary ion mass spectrometry, we show that Ga diffusion extends into the subsurface down to several tens of microns. X-ray diffraction patterns reveal minimal to no precipitation of wurtzite, resulting in limited infrared transmission loss after treatment. We report a monotonic increase in Vickers surface microhardness with increasing Ga concentration, reaching values more than double those of untreated windows. Future work will focus on optimizing this process and evaluating its effectiveness in enhancing the durability of ZnS windows under harsh environmental conditions.

**Keywords:** infrared windows; Ga<sub>2</sub>S<sub>3</sub>-ZnS system; mechanical properties of ceramics; transmission; doping profile



**Citation:** Soufiani, H.; Kostogiannes, A.; Rivero-Baleine, C.; Richardson, K.A.; Gaume, R. On the Surface Hardening of Zinc Sulfide Windows by Gallium Sulfide. *Materials* **2024**, *17*, 5622. <https://doi.org/10.3390/ma17225622>

Academic Editor: Rodrigo Moreno

Received: 2 October 2024

Revised: 30 October 2024

Accepted: 13 November 2024

Published: 18 November 2024



**Copyright:** © 2024 by the authors. Licensee MDPI, Basel, Switzerland. This article is an open access article distributed under the terms and conditions of the Creative Commons Attribution (CC BY) license (<https://creativecommons.org/licenses/by/4.0/>).

## 1. Introduction

Multispectral zinc sulfide (MS-ZnS) is a broadband optical ceramic window extensively used in the aviation and defense sectors. These types of applications require both high durability and transparency to maintain window integrity during operations. Pure ZnS exhibits polymorphism as it crystallizes into cubic (sphalerite), hexagonal (wurtzite), and numerous polytypic forms, referred to as hexagonality [1,2]. Due to the isotropy of its refractive index, sphalerite can be formed into scatter-free transparent ceramics suitable for optical imaging. Three distinct processes have been employed in the production of polycrystalline ZnS: vacuum sublimation, hot pressing (HP), and chemical vapor deposition (CVD). CVD-ZnS was found to have superior purity, enhanced density, and better optical homogeneity. In addition, yellow-colored CVD-ZnS can be further treated by hot isostatic pressing (HIP) to obtain a water-clear material, called multispectral ZnS (MS-ZnS), with an increased transmission over the 0.4 to 14 μm spectral range [2,3]. Although HIPing enhances transmission by stabilizing sphalerite and reducing porosity and hexagonality, it also causes grains to grow from a few microns to 20–200 μm [3,4], resulting in reduced mechanical strength [4–6] and overall performance [6–9]. Hence, multiple approaches have been used to strengthen CVD- and MS-ZnS through both surface and bulk modifications.

Surface treatments included film deposition [6,10,11], annealing under different atmospheres [6,10], and ion implantation [6,12,13]. However, most of these techniques have been discontinued because of unsatisfactory hardness enhancement, sample cracking, or transmission deterioration.

Bulk treatment techniques relying on solute strengthening [6,10,14], grain size refinement [6], ZnS-based composite fabrication via powder sintering [15,16], precipitation hardening [14], or development of glass ceramics [17] have also been considered. While solute strengthening and grain size refinement did not yield substantial improvements in the mechanical properties, ZnS-based composites showed promising results in terms of toughness, Young's modulus, and hardness. Notably, when examining sintered Ga<sub>2</sub>S<sub>3</sub>-ZnS ceramics, Dunn et al. [14] revealed a correlation between increasing Ga<sub>2</sub>S<sub>3</sub> content and decreasing grain size, resulting in substantial enhancements to both hardness and fracture toughness. The highest Vickers hardness of 427 kg·mm<sup>-2</sup> (4.18 GPa) was achieved for a composition containing 12 mol. % Ga<sub>2</sub>S<sub>3</sub> with a grain size of 6 μm. The group stated that several Ga<sub>2</sub>S<sub>3</sub>-ZnS solid solutions exhibited transmission properties comparable to that of pure ZnS; however, no experimental IR spectra were reported. Similarly, glass ceramics within the Ga-La-S-ZnS system have been explored as potential durable materials for long-wave infrared (LWIR) optics [17]. Studies showed that the ZnGa<sub>2</sub>S<sub>4</sub> crystallites embedded within the glass matrix increased hardness significantly, achieving values from 2.8 to 5.6 GPa, compared to 1.5 GPa for CVD-ZnS. However, the material was reported as opaque, likely due to factors such as extensive crystallization, oxygen contamination, and the presence of multiple phases [18].

The current study examines the effect of Ga diffusion on the microstructure, transmission, and hardness of MS-ZnS. To prevent oxidation, the process involved vacuum heat treatment of MS-ZnS blanks in the presence of Ga<sub>2</sub>S<sub>3</sub> powder. The temperature and mass ratio of the reactants,  $m_{\text{Ga}_2\text{S}_3} / m_{\text{ZnS}}$ , were carefully selected to retain the sphalerite-pure material and avoid the precipitation of wurtzite or tetragonal zinc thiogallate ZnGa<sub>2</sub>S<sub>4</sub> [14,19].

## 2. Experiment

Discs of MS-ZnS Cleartran™ (American Photonics, Sarasota, FL, USA), 25 mm in diameter and 2.50 mm thick with an average grain size of 40 μm, and gallium sulfide (Ga<sub>2</sub>S<sub>3</sub>) powder (99.99% Thermo Fisher Scientific, Waltham, MA, USA) were used. This powder was loaded into a small open-ended quartz tube and placed next to an MS-ZnS window in a larger quartz ampoule (Figure 1). The reaction chamber was then sealed under vacuum (200 mTorr). As part of the process optimization, the sealed ampoules were held at constant temperatures in the range of 800–900 °C for 1–4 weeks. For comparison, three Ga<sub>2</sub>S<sub>3</sub>-treated MS-ZnS coupons labeled as Samples #1, #2, and #3 with increasing  $m_{\text{Ga}_2\text{S}_3} / m_{\text{ZnS}}$  along with annealed MS-ZnS without Ga<sub>2</sub>S<sub>3</sub> were prepared under the same conditions of time and temperature. All samples were polished on both sides using 800 and 1200 grit pads, and surface was finished with a cloth pad and 0.5 μm alumina suspension. Secondary ion mass spectrometry (SIMS) was performed with an Adept 1010 Dynamic system (Chigasaki, Japan) equipped with an O<sub>2</sub><sup>+</sup> ion source. For quantification and correction for any variations in instrument parameters, changes in ion collections, sputtering yields, and ionization efficiencies [20], the relative sensitivity factors (RSFs) were obtained using three standards made by implanting 0.1, 0.5, and 1 at. % of <sup>69</sup>Ga ions into undoped MS-ZnS coupons at CuttingEdge ions LLC, Anaheim, CA, USA (see Appendix A). X-ray diffraction (XRD) analysis was carried out using a Panalytical diffractometer (Empyrean, Malvern, UK) equipped with a copper anticathode (Cu<sub>α1</sub> = 1.5406 Å). Diffraction patterns were collected over the range 20° < 2θ < 90° and fitted using HighScore Plus (version 4.5) software for phase identification. LaB<sub>6</sub> powder was used as an internal standard for all XRD analyses. A PerkinElmer fluorescence spectrometer LS 45 fitted to a Xe source was used to collect photoluminescence (PL) spectra across a wavelength range of 410–700 nm at room temperature. Infrared transmission was recorded over 400–7000 cm<sup>-1</sup> using a Fourier Transform Infrared (FTIR) Nicolet iS5 (Wilmington, MA, USA). The hardness of the samples was measured using a DUH-221S Shimadzu dynamic ultra-microhardness tester (Kyoto, Japan) fitted with a Vickers diamond pyramid (Kyoto, Japan). The microhardness reported for each sample was the average of 100 measurements obtained at room temperature under a load of 100 mN applied at 5.00 mN/s and held for 10 s.

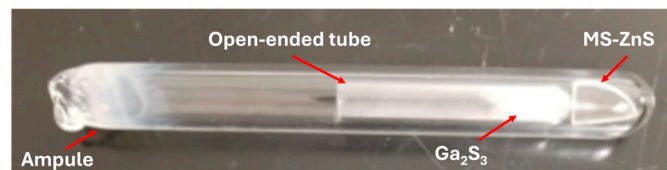


**Figure 1.**  $\text{Ga}_2\text{S}_3$  powder enclosed in a small tube to avoid direct contact with MS-ZnS. Both reactants are enclosed in a vacuum-sealed quartz ampoule to prevent oxidation.

### 3. Results and Discussion

#### 3.1. Microstructure and Ga Depth Profiling

The cross-sectional concentration profiles of Ga for Sample #3 are depicted in Figure 2a, demonstrating that  $\text{Ga}_2\text{S}_3$  has penetrated more deeply into the sample from both ends. The diffusion profile is nearly symmetrical with respect to the midplane of the sample as one might expect. Similarly, there is a slight non-uniformity in Ga doping across the surface of the same sample, as shown in Figure 2b, where the Ga depth profiles at three different locations are compared. Potential parameters that may play a role in Ga non-homogeneity are temperature irregularities, ZnS grain size uniformity, and orientation relative to the surface.

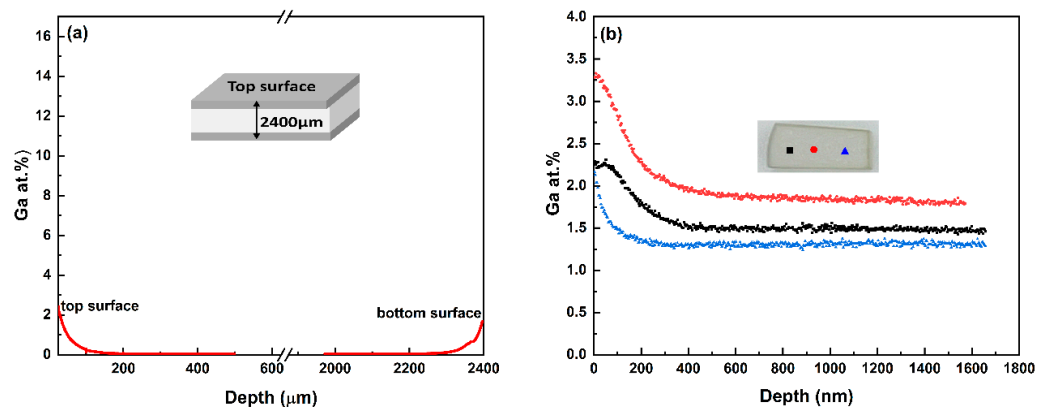


**Figure 2.** (a) Ga concentration profiles throughout the cross-section by SIMS 2D-image mode. (b) Ga depth profiles measured on the surface by SIMS depth profiling mode. These measurements were taken at three different locations 800  $\mu\text{m}$  apart, as shown on the inset, and are labeled red, black and blue for clarity.

X-ray diffraction patterns of the untreated, annealed, and Sample #3 coupons are presented in Figure 3. The square root of the intensities was plotted against  $2\theta$  to make peaks with smaller intensities more visible. The diffraction patterns exhibit similar characteristics, with minor variations in peak intensities and positions. As anticipated, the untreated MS-ZnS sample displays a pure cubic sphalerite (*s*) phase, characterized by an intense *s* (111) diffraction peak. Likewise, the heat-treated MS-ZnS coupon maintains the pure sphalerite structure, showing no transformation to the wurtzite (*w*) phase during annealing. This is evidenced by the absence of wurtzite diffraction peaks *w* (101) and *w* (102) at  $2\theta = 27.33^\circ$  and  $30.53^\circ$ , respectively. These findings align with previous study [21]. Conversely, as shown by Sample #3 patterns, the weak shoulder on the right side of the *s* (111) peak corresponds to the diffraction of the *w* (102) plane, which indicates the presence of some hexagonality [22,23].

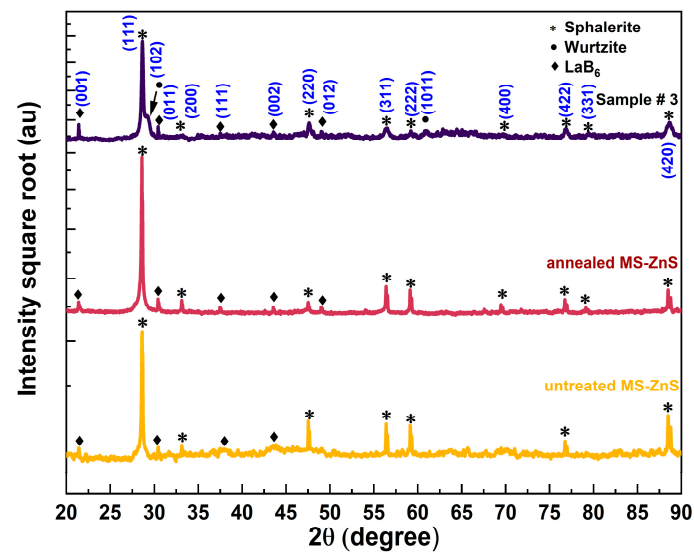
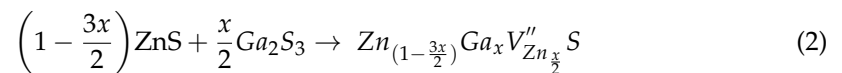


**Figure 3.** From bottom to top: X-ray diffraction patterns of untreated, annealed, and Sample #3 compared to *s* and *w* ZnS as per reference card #01-074-6110 and #01-089-2191, respectively, (see Appendix A for details).

Ueno et al. [24] reported the evolution of the unit cell parameter of Ga-bearing sphalerite as a function of the degree of cationic substitution,

$$R = Ga / (Ga + Zn) = 2x / (2 - x) \quad (1)$$

assuming the following substitutional mechanism:



where  $x$  designates the cation site fraction occupied by gallium. Our prior study has confirmed Ueno's findings and shown a shrinkage in lattice constant with increasing Ga concentration [25]. Table 1 summarizes the lattice parameters, phase content, and Ga content of the samples investigated here, as determined by XRD analysis.

**Table 1.** Lattice parameter, phase wt. %, and Ga content of untreated MS-ZnS, annealed MS-ZnS, and Ga<sub>2</sub>S<sub>3</sub>-treated MS-ZnS.

	Untreated MS-ZnS	Annealed MS-ZnS	Ga <sub>2</sub> S <sub>3</sub> -Treated MS-ZnS		
			Sample 1	Sample 2	Sample 3
Lattice parameter, (Å)	5.411(0)	5.411(0)	5.406(9)	5.405(1)	5.404(3)
Sphalerite phase, (wt. %)	100	100	~100	~100	~100
Wurtzite phase, (wt. %)	0	0	0	0	<0.1
Gallium content, $x$ , (at. %)	0	0	1.8	3.0	3.6

To further elucidate the mechanism of substitution, the PL spectra of untreated, annealed, and Sample #1 are compared in Figure 4. The peaks were adjusted through Lorentz deconvolution. The spectral profiles display distinct shapes, with their respective peaks showing varying positions and levels of intensity. All spectra exhibit a prominent peak at approximately 440 nm that can be attributed to the recombination of electron donors at sulfur vacancies with holes trapped at Zn vacancies [26]. The spectrum of annealed MS-ZnS shares similar spectral features with untreated MS-ZnS, with the exception of a broad band near 550 nm, which can be associated with structural defects resulting from annealing [27].

Interestingly, Sample #1 spectrum reveals two new bands centered at 475 nm and 610 nm, respectively, that are not observed in the annealed MS-ZnS spectrum despite both samples undergoing identical heating and cooling processes. These bands indicate the presence of Ga in ZnS [28,29] and have been linked to the association of  $Ga_{Zn}^{\bullet}$  and  $V_{Zn}''$  to form  $(V_{Zn}Ga_{Zn})^{\prime}$  centers (for 475 nm) and  $(V_{Zn}(Ga_{Zn})_2)$  complexes (for 610 nm) [28,30].

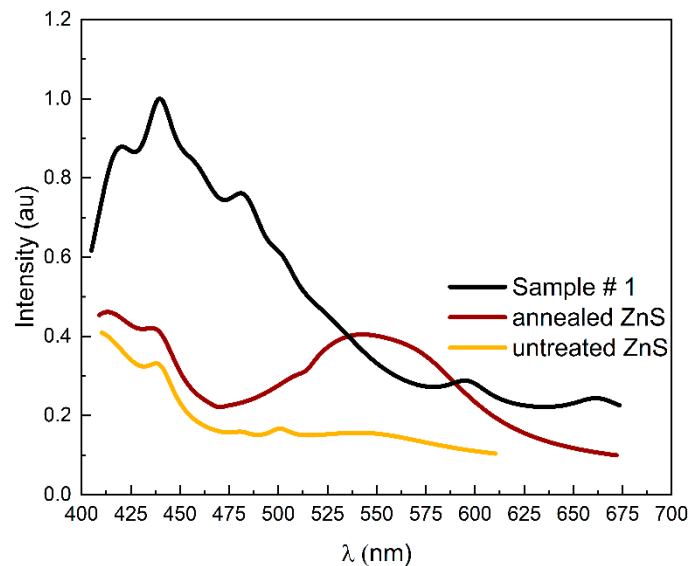


**Figure 4.** Photoluminescence spectra of untreated MS-ZnS, annealed MS-ZnS, and Sample #1 for 365 nm excitation.

### 3.2. Transmittance in IR

The untreated MS-ZnS, annealed MS-ZnS, and Sample #3 are transparent (Figure 5). Additionally, the infrared transmission of the annealed MS-ZnS is similar to that of untreated MS-ZnS (Figure 6) with a slight decrease that can be attributed to minor differences in the surface finish [23], whereas Sample #3 exhibits further loss due to light scattering. A similar trend was observed by Dunn et al. when co-sintering ZnS with  $Ga_2S_3$  [14]. No absorption band is introduced by annealing nor after Ga diffusion. The non-uniform distribution of Ga in both radial and cross-sectional directions, as evidenced by XRD and SIMS analyses, is likely the primary cause of scattering. This phenomenon occurs due to spatial variations in the refractive index at the scale of the wavelength. Additionally, potential differences in lattice and grain boundary diffusion coefficients for Ga in ZnS may contribute to scattering at the grain level.



**Figure 5.** From left to right: untreated, annealed, and Sample #3.

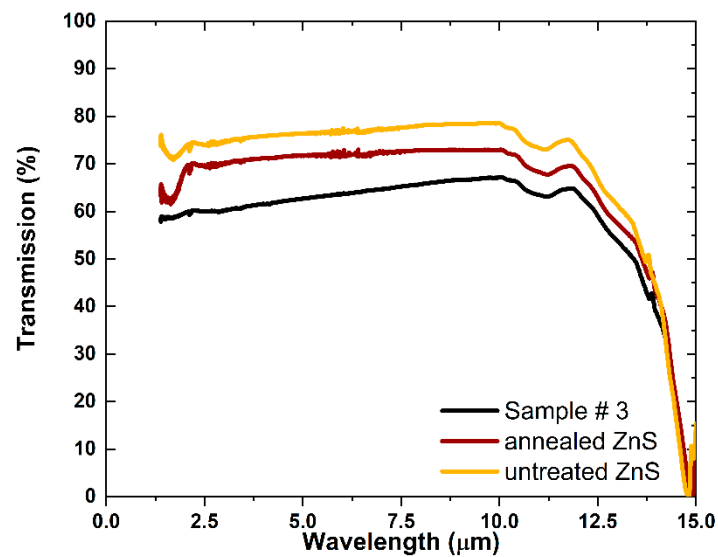


**Figure 6.** Infrared transmission spectra of untreated MS-ZnS (yellow), annealed MS-ZnS (red), and Sample #3 (black). The thicknesses of these samples are similar, measuring 2.49, 2.44, and 2.40 mm, respectively.

### 3.3. Hardness

Hardness quantifies the resistance of a material to localized plastic deformation under a fixed load and is often used as an estimate of mechanical strength. The degree of plastic deformation in polycrystalline materials varies depending on factors such as the sliding direction, dislocation density, and the ratio of grain size to indenter size [31,32]. In this study, microhardness measurements were performed under typical conditions to measure the indentation diagonals [33] as accurately as possible and were averaged over 100 locations on the sample to improve the statistics. Additionally, tests that generated cracks (fractures) were discarded from the analysis.

The histogram in Figure 7a shows the results of one hundred Vickers microhardness tests conducted on each sample. The data indicate that untreated and annealed MS-ZnS have comparable hardness, with overlapping distributions and no notable differences in the average microhardness values or standard deviations. In contrast, Sample #3 demonstrates enhanced hardness, reaching up to 2.2 times that of untreated MS-ZnS. A comparison between our experimental data and Dunn's group findings is presented in Figure 7b. Samples #1, #2, and #3 compositions are within the sphalerite-pure region, suggesting that the observed strengthening in these specimens is attributable to solute strengthening despite the presence of hexagonality or wurtzite as revealed by XRD analysis in (Figure 3). This implies that Ga may have initiated the nucleation of a small amount of wurtzite, insufficient to impose a hardening mechanism. The FTIR results further support this conclusion. This outcome differs from Dunn et al.'s experimental data [14], where strengthening results from zinc thiogallate ( $ZnGa_2S_4$ ) precipitation, as all sample compositions fall within the two-phase region where sphalerite and tetragonal phases coexist. The significance of our work lies in demonstrating that diffusing Ga into the MS-ZnS matrix has a substantial hardening effect while maintaining a single, optically transparent, sphalerite phase. Additionally, Figure 8, which graphically presents the data from Table 2, illustrates an important finding: The microhardness linearly increases with the square root of Ga concentration, aligning with Fleisher's mechanism. This observation is consistent with several previous studies [34–36] that demonstrated the proportionality between the stress field intensity in slip planes and solute concentration, which impedes dislocation motion [35], thereby strengthening the material.



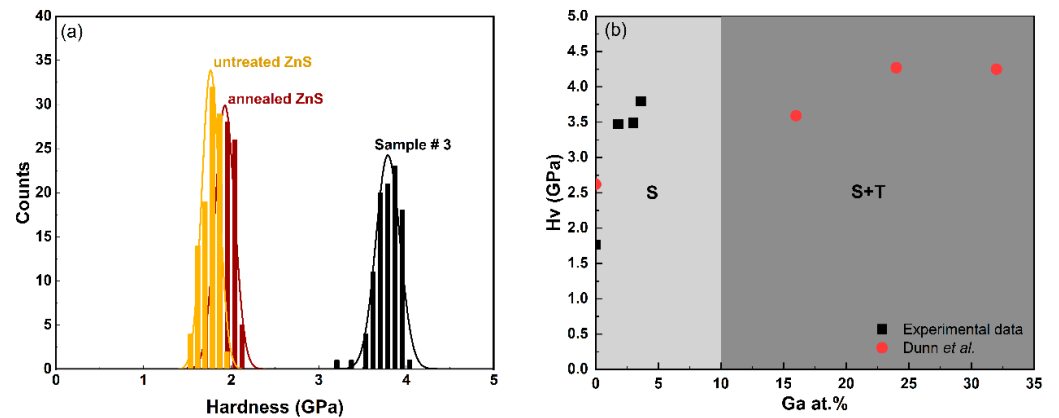


**Figure 7.** (a) Vickers microhardness distribution of untreated MS-ZnS, annealed MS-ZnS, and Sample #3. (b) Average microhardness values of Samples #1, #2, and #3 obtained by  $\text{Ga}_2\text{S}_3$ -treatment (this work) compared to co-sintered  $\text{Ga}_2\text{S}_3$ -ZnS ceramics (from [14]). The single sphalerite (S) phase and two-phase sphalerite + tetragonal (S + T) domains are both represented in this figure to highlight the difference in hardness improvement one can obtain from cationic substitution (single-phase solute strengthening) and precipitation hardening (presence of two-phases). The latter comes at the expense of transparency due to scattering.

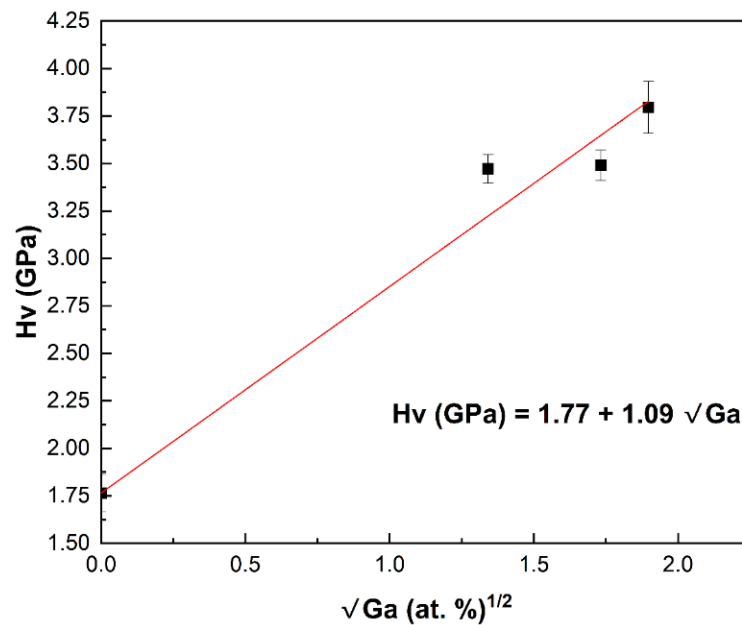


**Figure 8.** Linear evolution of hardness with  $\sqrt{\text{Ga}}$  concentration in  $\text{Ga}_2\text{S}_3$ -treated MS-ZnS.

**Table 2.** Results of Vickers microhardness indentation on MS-ZnS, annealed, and of Samples #1, #2, and #3. The data represent the average value ( $H_v$ ) and standard deviation ( $\sigma_{H_v}$ ) for 100 tests on each sample.

Ga (at. %)	$H_v$ (GPa)	$\sigma_{H_v}$ (GPa)
0 (untreated)	1.77	0.10
0 (annealed)	1.92	0.11
1.8	3.47	0.08
3.0	3.49	0.08
3.6	3.80	0.14

#### 4. Conclusions

Diffusing Ga<sub>2</sub>S<sub>3</sub> into multispectral-grade ZnS by thermal vapor deposition resulted in substantial improvements in surface microhardness, with values more than doubling compared to untreated windows (3.80 GPa for 3.6 at% Ga-doping versus 1.77 GPa for untreated window). The observed linear increase in hardness with the square root of Ga concentration aligns with Fleisher's mechanism, indicating solute strengthening as the primary hardening mechanism. Importantly, this hardening is achieved without inducing significant phase changes, thus preserving broadband transmission and minimizing infrared transmission loss. Although promising, this approach will require further investigation to assess microstructural changes, long-term mechanical durability, and optical performance under operational conditions. Additionally, optimizing the diffusion process will be essential to ensure uniform strengthening, especially in larger optics.

**Author Contributions:** Conceptualization, H.S. and R.G.; Methodology, H.S., R.G., C.R.-B. and K.A.R.; Investigation, H.S.; Resources, R.G., A.K., C.R.-B. and K.A.R.; Data curation, H.S. and A.K.; Writing—original draft, H.S.; Writing—review & editing, R.G.; Supervision, R.G. All authors have read and agreed to the published version of the manuscript.

**Funding:** Funded under Lockheed Martin-University Engagement Program grant number [00006199].

**Institutional Review Board Statement:** Not applicable.

**Informed Consent Statement:** Not applicable.

**Data Availability Statement:** The original contributions presented in this study are included in the article. Further inquiries can be directed to the corresponding author.

**Conflicts of Interest:** Author Clara Rivero-Baleine was employed by the company Lockheed Martin Corporation. The remaining authors declare that the research was conducted in the absence of any commercial or financial relationships that could be construed as a potential conflict of interest.

#### Appendix A

##### Appendix A.1. SIMS Data Analysis

Figure A1 shows the SIMS spectrum of Sample #3 measured on its surface. The peaks of <sup>69</sup>Ga and <sup>71</sup>Ga appear very intense, clearly showing that gallium sulfide was deposited on the surface of the sample.

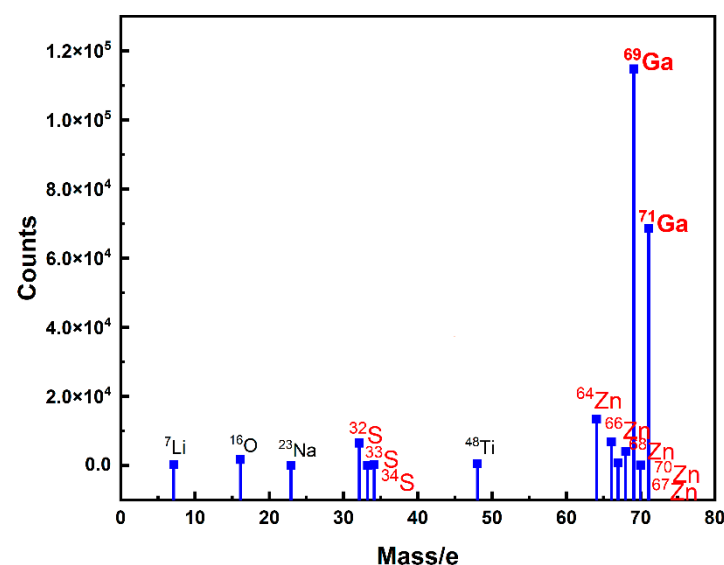


Figure A1. SIMS spectrum Sample #3 collected from the surface.



RSF values for  $^{69}\text{Ga}$  in ZnS were calculated using an integration approach similar to [37] (Table A1). RSF converts the count rates to atom density [38–40] (Equation (A1)):

$$C_{69\text{Ga}} \text{ (at.\%)} = \frac{1}{\rho} \frac{I_{69\text{Ga}}}{I_{64\text{Zn}}} \times \text{RSF} \text{ (at}\cdot\text{cm}^{-3}) \times 100 \quad (\text{A1})$$

Here, the factor  $1/\rho$  allows for the conversion of concentrations in  $(\text{at}\cdot\text{cm}^{-3})$  to  $(\text{at. \%})$ . The experimental density of pure MS-ZnS  $\rho = 5.05248 \times 10^{22} \text{ (at}\cdot\text{cm}^{-3})$  was adopted by considering both the standards and all samples in this study as dilute solid solutions [38–40]. Then, knowing the concentration of  $^{69}\text{Ga}$  in the standards and selecting  $^{64}\text{Zn}$  as the matrix major isotope, a calibration curve of concentration versus normalized  $^{69}\text{Ga}$  intensity ( $\frac{I_{69\text{Ga}}}{I_{64\text{Zn}}}$ ) can be established and fitted to a linear model (Figure A2).

$$C_{69\text{Ga}} \text{ (at.\%)} = 0.118 \times \frac{I_{69\text{Ga}}}{I_{64\text{Zn}}} \quad (\text{A2})$$

Using the SIMS results of the  $\text{Ga}_2\text{S}_3$ -treated samples, the concentration of  $^{69}\text{Ga}$  is deduced according to Equation (A2) and converted into the total gallium content by taking the natural abundances of  $^{69}\text{Ga}$ ,  $A_{69\text{Ga}} = 60.10\%$  [41] into account:

$$C_{\text{Ga}} \text{ (at.\%)} = \frac{C_{69\text{Ga}} \text{ (at.\%)}}{A_{69\text{Ga}}} \quad (\text{A3})$$

**Table A1.** RSF values of  $^{69}\text{Ga}$  in ZnS over the concentration range 0.1 to 1 (at. %).

$^{69}\text{Ga}$ -Implanted ZnS Standards (at. %)	0.1	0.5	1.0
RSF ( $\text{at}\cdot\text{cm}^{-3}$ )	$7.52 \times 10^{19}$	$6.68 \times 10^{19}$	$5.76 \times 10^{19}$

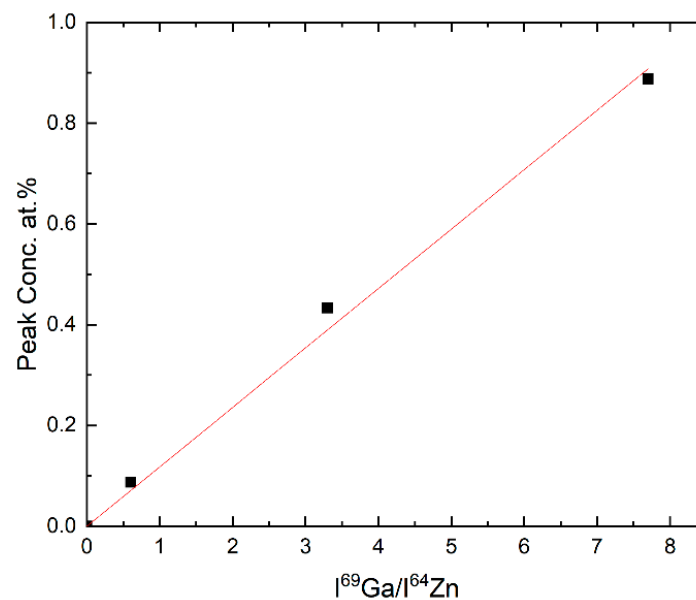


**Figure A2.** Calibration curve of  $^{69}\text{Ga}$  concentration versus the experimental SIMS intensity ratio  $I^{69\text{Ga}}/I^{64\text{Zn}}$ .

#### Appendix A.2. XRD Data

The X-ray diffraction patterns of all samples are presented in Figure A3. The square root of the intensities was plotted against  $2\theta$  to make peaks with smaller intensities more visible. X-ray diffraction patterns of  $\text{LaB}_6$ ,  $s$ , and  $w$  ZnS are included for comparison.

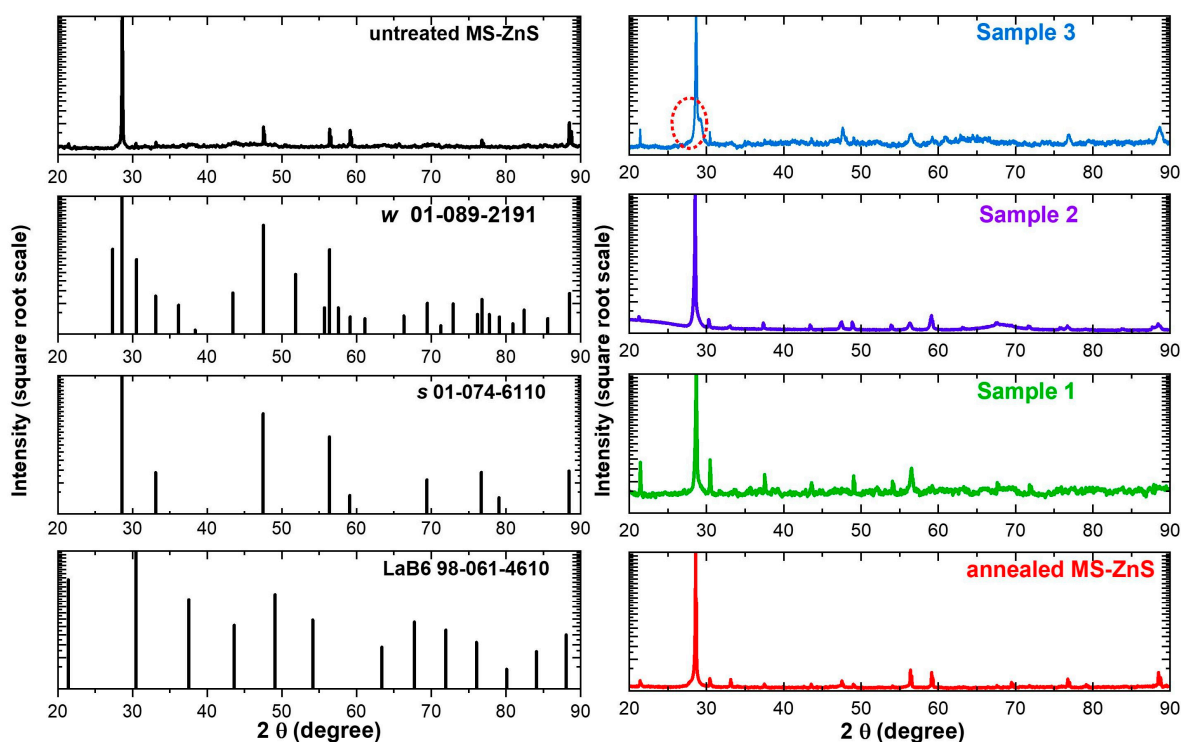


**Figure A3.** From bottom to top: X-ray diffraction patterns of LaB<sub>6</sub>, *s*, and *w* ZnS (as per reference card #98-061-4610, #01-074-6110, and #01-089-2191, respectively), and untreated ZnS (left). From bottom to top: X-ray diffraction patterns of annealed ZnS, Samples #1, #2, and #3 (right). The red circle shown on the pattern of sample #3 highlights the broadening of the *s* (111) due some hexagonality.

## References

- Steinberger, I.T.; Kiflawi, I.; Kalman, Z.H.; Mardix, S. The stacking faults and partial dislocations involved in structure transformations of ZnS crystals. *Philos. Mag.* **1973**, *27*, 159–175. [\[CrossRef\]](#)
- Karaksina, E.V.; Gracheva, T.A.; Shevarenkov, D.N. Structural defects in CVD ZnS. *Inorg. Mater.* **2010**, *46*, 6–10. [\[CrossRef\]](#)
- Yashina, E.V. Preparation and properties of polycrystalline ZnS for IR applications. *Inorg. Mater.* **2003**, *39*, 663–668. [\[CrossRef\]](#)
- Shchurov, A.F.; Perevoshchikov, V.A.; Gracheva, T.A.; Malygin, N.D.; Shevarenkov, D.N.; Gavriushchuk, E.M.; Ikonnikov, V.B.; Yashina, E.V. Structure and Mechanical Properties of Polycrystalline Zinc Sulfide. *Inorg. Mater.* **2004**, *40*, 96–101. [\[CrossRef\]](#)
- Harris, D.C. Development of hot-pressed and chemical-vapor-deposited zinc sulfide and zinc selenide in the United States for optical windows. In *Defense and Security Symposium*; SPIE: Orlando, FL, USA, 2007. [\[CrossRef\]](#)
- Taylor, R.; Lefebvre, M.; Price, P. *Erosion Resistant FLIR Windows: Colorless ZnS*; Air Force Wright Aeronautical Laboratories: Dayton, OH, USA, 1984.
- Musikant, S.; Savage, J.A.; Marsh, K.J. A Materials Study To Find An Advanced Optical Window Material For 8 to 12  $\mu\text{m}$  Airborne Applications. In *Proceedings of the 25th Annual Technical Symposium*, San Diego, CA, USA, 26 February 1982; pp. 35–37. [\[CrossRef\]](#)
- Hackworth, J.V. A mechanistic investigation of the rain erosion of infrared transmitting materials at velocities to Mach 2. In *On Erosion by Solid and Liquid Impact*; Cavendish Laboratory, University of Cambridge: Cambridge, UK, 1979; pp. 10-1–10-12.
- Tustison, R.; Gentilman, R. Current and emerging materials for LWIR external windows. In *Proceedings of the 32nd Annual International Technical Symposium on Optical and Optoelectronic Applied Science and Engineering*, San Diego, CA, USA, 15–18 August 1989. [\[CrossRef\]](#)
- Dibenedetto, B.A.; Pappis, J.; Capriulo, A.J. *Chemical Vapor Deposition of Multispectral Windows*; U.S. Department of Energy Office of Scientific and Technical Information: Washington, DC, USA, 1973.
- Guo, G.Z.L.J.; Zheng, Z.L.X. Application of diamond-like carbon film as protection and antireflection coatings of ZnS elements. *Opt. Eng.* **1994**, *33*, 1330–1333.
- Wu, R.L.C.; McCormick, A.W.; Pronko, P.P. Surface hardening of ZnSe and ZnS/ZnSe optical materials by implantation of 1MeV hydrogen ions. *Nucl. Instrum. Methods Phys. Res. Sect. B* **1991**, *59*, 1232–1235. [\[CrossRef\]](#)
- Klocek, P.; Swec, D.M.; Mirtich, M.J. Diamondlike Carbon Protective Coatings For Optical Windows. In *Proceedings of the SPIE 1989 Technical Symposium on Aerospace Sensing*, Orlando, FL, USA, 27–31 March 1989. [\[CrossRef\]](#)

14. Dunn, B.; Ardell, A.J. Precipitation hardening of IR ZnS Ceramics. In *SPIE 1990*; Volume 13. Available online: <https://apps.dtic.mil/sti/tr/pdf/ADA265184.pdf> (accessed on 12 November 2024).
15. Xue, L.A.; Farquhar, D.S.; Noh, T.W.; Sievers, A.J.; Raj, R. Optical and mechanical properties of zinc sulfide diamond composites. *Acta Metall. Mater.* **1990**, *38*, 1743–1752. [[CrossRef](#)]
16. Fujii, A.; Wada, H.; Shibata, K.-I.; Nakayama, S.; Hasegawa, M. Diamond-ZnS composite infrared window. In Proceedings of the Aerospace/Defense Sensing, Simulation, and Controls, Orlando, FL, USA, 16–20 April 2001; pp. 206–217. [[CrossRef](#)]
17. McCloy, J.S.; Riley, B.J.; Pierce, D.A. Infrared-transparent glass ceramics: An exploratory study. *J. Non-Cryst. Solids* **2015**, *410*, 160–173. [[CrossRef](#)]
18. Tustison, R.W.; McCloy, J.S.; Riley, B.J.; Pierce, D.A.; Johnson, B.R.; Qiao, A.; Zelinski, B.J. Infrared-transmitting glass-ceramics: A review. In Proceedings of the Window and Dome Technologies and Materials XIII, Baltimore, MA, USA, 1–3 May 2013.
19. Zhang, J.; Chen, W.; Dunn, B.; Ardell, A. Phase diagram studies of ZnS systems. In Proceedings of the 32nd Annual International Technical Symposium on Optical and Optoelectronic Applied Science and Engineering, San Diego, CA, USA, 15–18 August 1988; Volume 968. [[CrossRef](#)]
20. Cabri, L.J.; Momahon, G. SIMS analysis of sulfide minerals for Pt and Au methodology and relative sensitivity factors RSF. *Can. Mineral.* **1995**, *33*, 349–359.
21. McCloy, J.S.; Tustison, R.W. *Chemical Vapor Deposited Zinc Sulfide*; SPIE Press: Bellingham, WA, USA, 2013. [[CrossRef](#)]
22. Kimi, M.; Yuliati, L.; Shamsuddin, M. Preparation of high activity Ga and Cu doped ZnS by hydrothermal method for hydrogen production under visible light irradiation. *J. Nanomater.* **2015**, *2015*, 195024. [[CrossRef](#)]
23. McCloy, J.S. Properties and Processing of Chemical Vapor Deposition of ZnS. Ph.D. Thesis, The University of Arizona, Tucson, AZ, USA, 2008.
24. Ueno, T.; Scott, S.D. Phase relations in the system Zn-Ga-S at 900 degrees C and 800 degrees C. *Can. Mineral.* **1995**, *33*, 129–136.
25. Soufiani, H.; Kostogiannes, A.; Rivero-Baleine, C.; Richardson, K.A.; Gaume, R. Solute strengthening of multispectral ZnS windows by vapor transport of Ga<sub>2</sub>S<sub>3</sub>. In Proceedings of the Window and Dome Technologies and Materials XVII, Orlando, FL, USA, 4 May 2023; Volume 12518. [[CrossRef](#)]
26. Shahid, R.; Toprak, M.; Soliman, H.; Muhammed, M. Low temperature synthesis of cubic phase zinc sulfide quantum dots. *Open Chem.* **2012**, *10*, 54–58. [[CrossRef](#)]
27. Grasser, R.; Scharmann, A.; Schwedes, W. Further effects of high temperature annealing on the photoluminescence of an ultra high pure ZnS crystal. *Eur. Phys. J. B* **1977**, *28*, 247–253. [[CrossRef](#)]
28. Bacherikov, Y.Y.; Vorona, I.P.; Optasyuk, S.V.; Rodionov, V.E.; Stadnik, A.A. Certain features of Ga diffusion in ZnS powders. *Semiconductors* **2004**, *38*, 987–991. [[CrossRef](#)]
29. Bacherikov, Y.Y.; Kitsyuk, N.V.; Optasyuk, S.V.; Stadnik, A.A. The Effect of Pressing on the Luminescent Properties of ZnS:Ga. *Semiconductors* **2005**, *39*, 316–319. [[CrossRef](#)]
30. Il'Ina, M.A.; Gutan, V.B.; Gurvich, A.M. Defect association and nature of the emission centers for gallium-activated zinc sulfide. *J. Appl. Spectrosc.* **1971**, *14*, 612–616. [[CrossRef](#)]
31. DTownsend, D.; Field, J.E. Fracture toughness and hardness of zinc sulphide as a function of grain size. *J. Mater. Sci.* **1990**, *25*, 1347–1352. [[CrossRef](#)]
32. Flom, D.G.; Komanduri, R. Some indentation and sliding experiments on single crystal and polycrystalline materials. *Wear* **2002**, *252*, 401–429. [[CrossRef](#)]
33. Clinton, D.J.; Morrell, R. Hardness testing of ceramic materials. *Mater. Chem. Phys.* **1987**, *17*, 461–473. [[CrossRef](#)]
34. Gao, F. Hardness of cubic solid solutions. *Sci. Rep* **2017**, *7*, 40276. [[CrossRef](#)]
35. Rao, S.; Babu, V. Microhardness studies in alkali halide mixed crystals. *Pramana* **1978**, *11*, 149–157.
36. Ali, N.; Zhang, L.; Liu, D.; Zhou, H.; Sanaullah, K.; Zhang, C.; Chu, J.; Nian, Y.; Cheng, J. Strengthening mechanisms in high entropy alloys: A review. *Mater. Today Commun.* **2022**, *33*, 104686. [[CrossRef](#)]
37. *ASTM E1505-92*; Standard Guide for Determining SIMS Relative Sensitivity Factors From Ion Implanted External Standards. ASTM: West Conshohocken, PA, USA, 2001.
38. Laufer, A.; Volbers, N.; Eisermann, S.; Potzger, K.; Geburt, S.; Ronning, C.; Meyer, B.K. Determination of secondary ion mass spectrometry relative sensitivity factors for polar and non-polar ZnO. *J. Appl. Phys.* **2011**, *110*, 94906. [[CrossRef](#)]
39. Wilson, R.G.; Novak, S.W. Systematics of secondary-ion-mass spectrometry relative sensitivity factors versus electron affinity and ionization potential for a variety of matrices determined from implanted standards of more than 70 elements. *J. Appl. Phys.* **1991**, *69*, 466–474. [[CrossRef](#)]
40. Stevie, F.A.; Wilson, R.G. Relative sensitivity factors for positive atomic and molecular ions sputtered from Si and GaAs. *J. Vac. Sci. Technol. A Vac. Surf. Film.* **1991**, *9*, 3064–3070. [[CrossRef](#)]
41. Stevie, F.A. *Secondary Ion Mass Spectrometry Applications for Depth Profiling and Surface Characterization*; Momentum Press®, LLC.: New York, NY, USA, 2016.

**Disclaimer/Publisher's Note:** The statements, opinions and data contained in all publications are solely those of the individual author(s) and contributor(s) and not of MDPI and/or the editor(s). MDPI and/or the editor(s) disclaim responsibility for any injury to people or property resulting from any ideas, methods, instructions or products referred to in the content.